Customization and improvement of the LbCas12a-crRNA system for efficient gene targeting in plants

Tien Van Vu[1,2,5,*], Duong Thi Hai Doan[1,5], Mil Thi Tran[1,3,5], Yeon Woo Sung[1], Young Jong Song[1], Jae-Yean Kim[1,4,*]

[1]Division of Applied Life Science (BK21 FOUR Program), Plant Molecular Biology and Biotechnology Research Center, Gyeongsang National University, Jinju 660-701, Republic of Korea.

[2]National Key Laboratory for Plant Cell Biotechnology, Agricultural Genetics Institute, Km 02, Pham Van Dong Road, Co Nhue 1, Bac Tu Liem, Hanoi 11917, Vietnam.

[3]Crop Science and Rural Development Division, College of Agriculture, Bac Lieu University, Bac Lieu-97000, Vietnam.

[4]Division of Life Science, Gyeongsang National University, 501 Jinju-daero, Jinju 52828, Republic of Korea.

[5]These authors contributed equally as co-first authors: Tien Van Vu, Duong Thi Hai Doan, Mil Thi Tran.

*Correspondence: Jae-Yean Kim: kimjy@gnu.ac.kr (ORCID ID: 0000-0002-1180-6232). Tien Van Vu: tienvu.agi@gmail.com (ORCID: 0000-0002-6369-7664).

Keywords: LbCas12a; Gene targeting; Gene editing; Homology-directed repair; SpCas9; geminiviral replicon.

Running title: LbCas12a-based gene targeting in tomato.

Word count: 5131

Abstract: 149/150

Number of Main Figures: 05

Number of Supplementary Figures: 12

Number of Supplementary Tables: 08

Abstract

Plant gene targeting (GT) can be utilized to precisely replace up to several kilobases of a plant genome. Recent studies using the powerful clustered regularly interspaced short palindromic repeats (CRISPR) and CRISPR-associated (Cas) nucleases significantly improved plant GT efficiency. However, GT for loci without associated selection markers is still inefficient. We previously utilized *Lachnospiraceae bacterium* Cas12a (LbCas12a) in combination with a replicon for tomato GT and obtained high GT efficiency with some selection markers. In this study, we customize and advance our GT system by using a temperature-tolerant LbCas12a (ttLbCas12a) in combination with various crRNA forms and chemical treatments to suppress the canonical non-homologous end-joining pathway in tomato. Our work demonstrates the significance of the selection of gene scissors, the appropriate design of LbCas12a gRNAs, the use of chemical treatments, and the establishment of favorable experimental conditions for further enhancement of plant HDR to enable efficient GT in tomato.

Introduction

Plant gene targeting (GT) was first reported in 1988 by Paszkowski and coworkers, although that study only obtained low efficiency of targeting[1], and GT usually requires at least one associated selection marker for the practical achievement of GT events[2, 3]. Without any

targeted DSB and with an antibiotic selection marker, the GT efficiency remained extremely low[4]. An important improvement was made to plant GT by introducing DSBs at the targeted sites using a preinserted I-SceI recognition sequence; this approach ultimately enhanced the GT efficiency up to hundreds of fold[5, 6], but the efficiency was still low (i.e., up to 1.83%) and required two selection markers. The subsequent development of the first, second and, especially, third generations of site-directed nucleases (SDNs) has revolutionized precision gene editing technology with the easy customization of targeted DSBs at any site of interest for exchanging donor DNA templates[7-9].

Until recently, SDN-based GT efficiency has been significantly enhanced through combinations of SDN complexes and geminiviral replicons, which are autonomously replicative vectors for supplying high doses of homologous DNA template to DSB repair foci[10-13]. Further improvement of plant GT was also possible with the suppression of cNHEJ[14-17] or activation of HDR mechanisms[18] using biological approaches or chemical treatments. Nevertheless, chemical treatments have not been heavily studied in conjunction with CRISPR/Cas-based GT in plants. Overall, the practical GT efficiency with allele-associated selection markers was approximately 10% in most of the "accessible" plants and considerably lower in difficult systems or those with targeted loci lacking selection markers[3]. Therefore, continuous improvement of plant GT remains necessary, especially for applications in less accessible plants.

Our previous work showed the significant improvement of plant GT using geminiviral replicons and LbCas12a, rather than SpCas9[12]. More importantly, the activity of LbCas12a nucleases was more temperature-dependent than that of SpCas9[12, 19]. Recently, a temperature-tolerant LbCas12a mutant (D156R), known as ttLbCas12a, which exhibited significantly improved

cleavage activity and hence gene targeting efficiency, was reported with conventional approaches in *Arabidopsis*[20, 21]. However, further characterization of ttLbCas12a for somatic cell-based GT systems, especially in combination with DNA replicons, has not been undertaken. We hypothesized that ttLbCas12a could be utilized to further improve our replicon-based plant GT system through appropriate customization of its nuclease-crRNA complexes. Chemical treatment for suppressing cNHEJ or activating HDR pathways was also tested and validated for practical GT applications in tomato. In this report, we describe a further comparison of LbCas12a and SpCas9 in inducing GT at the SlANT1 locus. Subsequently, extensive characterization of ttLbCas12a in comparison with LbCas12a is shown at the SlANT1, SlHKT1;2, and SlEPSPS1 loci with or without allele-associated selection markers. Our work demonstrates the significance of utilizing appropriate design of CRISPR/Cas-crRNA complexes, chemical treatments, and favorable experimental conditions to further enhance plant HDR for efficient GT in tomato.

Results

NU7441 treatment enhances LbCas12a-based GT efficiency

A plant genomic DNA DSB may be repaired by two major competing mechanisms, namely, cNHEJ and HDR. The GT approach is based on the HDR mechanism; therefore, to increase its efficacy, blocking the cNHEJ pathway is a good option[3]. A number of studies have been published regarding the uses of chemical treatments for blocking cNHEJ to enhance GT efficiency in mammals[16, 17, 22, 23]. However, only limited information regarding the applications of the chemicals to plant GT is currently available. Therefore, we selected SCR7 (an inhibitor of DNA ligase IV), NU7441 (a DNA-dependent protein kinase (DNA-PKcs) inhibitor), and

KU0060648 (a dual inhibitor of DNA-PKcs and phosphatidylinositol-3 kinase (PI-3K)) to determine their effects on plant GT. Although no plant homolog of animal DNA-PKcs has been identified to date, alternative DNA-dependent protein kinases might be involved in DNA DSB repair in plants. Previously, a replicon-based CRISPR/Cas-mediated targeted DNA insertion system was successfully developed with SlANT1 as a visible marker[10, 12]. We used SpCas9 (pTC217) and LbCas12a (pHR01 and pMR01) carrying GT vectors to assess the effects of chemical treatments.

During the GT reaction performed using the SpCas9-based pTC217 vector, treatment with the DNA ligase IV inhibitor led to an improvement in the GT efficiency compared to the mock control (Fig. 1a, upper panel). The GT efficiency was increased to 34% with the treatments of either 10 or 50 µM SCR7 compared to the mock 0 µM treatment or the 1 µM SCR7 treatment. However, Fisher's LSD test for comparison of the GT efficiency between the treated concentrations and the mock control did not return significant p-values to determine whether the GT enhancement was strong enough (Fig. 1a, upper panel). The data indicate that 10 µM SCR7 was the best concentration for SpCas9-based GT in tomato. By contrast, the LbCas12a-based pHR01 construct exhibits a decreasing trend from the mock control to the highest SCR7 concentration. There were mild GT efficiency changes among the mock and 1 or 10 µM SCR7 treatments. Nevertheless, the GT efficiency was dramatically reduced to 4.140 ± 0.66% at 50 µM SCR7 from 6.95 ± 0.91% in the mock treatment (68% reduction) (Fig. 1a, bottom panel).

To test the impacts of NU7441 and KU0060648 on CRISPR/Cas-based GT in tomato, we employed both single and multiple replicon systems to carry the SpCas9 or LbCas12a constructs. In the case of SpCas9, the GT efficiency was slightly increased (Fig. 1b, top panel)

when 0.2 µM KU0060648 or 1 µM NU7441, which were within the optimal concentration ranges tested in human cells[16], was applied to NSEL medium (Supplemental Fig. 1) and incubated from days 3 to 8 post-transformation. However, pairwise comparison resulted in p-values that were not small enough to reject the null hypothesis. A similar situation also occurred for the LbCas12a-based single replicon, although NU7441 treatment led to a smaller p-value. In this case, 1 µM NU7441 treatment resulted in GT efficiency at 11.07 ± 1.50% compared to 7.17 ± 1.67% of that of the mock control, which represented a 1.54-fold enhancement (Fig. 1b, middle panel). The effect is considerably more clear with NU7441 treatment using the LbCas12a-based multiple replicon system. Blocking cNHEJ with 1 µM NU7441 significantly increased the multireplicon-based GT efficiency from 11.01 ± 0.93% in the mock control to 15.89 ± 1.15%, representing an approximately 1.44-fold change (Fig. 1b, bottom panel). There was almost no GT efficiency change in the case of KU0060648 treatment with pMR01.

Silver nitrate treatment enhances GT efficiency and purple shoot regeneration

Recently, polyamines, such as putrescine, spermidine, and spermine, were shown to enhance HDR by facilitating RAD51-mediated homologous strand annealing and synaptic complex formation[24]. We added 1 mM putrescine, spermidine, or spermine to the NSEL medium and incubated the transformed explants for 5 days after cocultivation with agrobacteria carrying the pMR01 plasmid. In contrast to the observations made in animals, no improvement in GT efficiency was achieved by any of the polyamines in the two replicates. In fact, the GT efficiency was reduced with supplementation with longer chain polyamines (i.e., spermidine and spermine) (Supplemental Fig. 2). We also observed a higher proliferation of the purple GT calli

and a delay in shoot formation from the explants treated with spermidine or spermine compared to the mock control. We surmised that direct supplementation with synthetic polyamines, especially spermidine and spermine, at high concentrations might not facilitate organ regeneration.

In tissue culture, silver nitrate ($AgNO_3$) was used as a regulator of ethylene action[25] that resulted in the enhancement of somatic embryogenesis[26, 27]. Silver nitrate was also shown to stimulate the activity of arginine decarboxylase (ADC; EC 4.1.1.9), one of the key enzymes of putrescine biosynthesis[28]. We hypothesized that adding $AgNO_3$ into the tissue culture media may help enhance polyamine synthesis and somatic embryogenesis. Using the pMR01 vector for this experiment, we treated the transformed explants with 30 µM $AgNO_3$ for 5 days on NSEL medium. In two replicates, we observed a significant increase in the number of purple GT spots per explant compared to that of the mock control (Supplemental Fig. 3a). More importantly, the addition of $AgNO_3$ stimulated shoot regeneration from purple calli (Supplemental Fig. 3b), although it required more time due to the enhancement of callus proliferation.

LbCas12a-based GT is superior to the SpCas9-based GT

In our previous report, LbCas12a was shown to mediate GT more effectively than the SpCas9 system. The comparisons were conducted at the SlANT1 locus under various experimental conditions[12]. However, the comparison using the replicon-based pTC217 and pHR01 constructs might have flawed parameters, such as slightly different SSN-mediated binding and cutting sites and donors. Furthermore, the promoter and terminator driving the expression of SpCas9 and LbCas12a might also contribute to the differences. To better characterize and compare the GT performance of SpCas9 and LbCas12a, we designed a GT system with SlANT1 cutting sites that

are accessible to both nucleases (Fig. 2a and Supplemental Fig. 4) and the same promoter and terminator to drive the transcription of Cas nucleases. The comparisons were conducted using single gRNA (sgR2^{ANT1} vs. crR1.23^{ANT1} and crR3.20^{ANT1}, sgR3^{ANT1} vs. crR3.23^{ANT1}) (Fig. 2b and Data S1). Each of the GT tools was expressed from both the replicon and T-DNA to compare the GT efficiency of the two delivery methods (Fig. 2b). Our data demonstrate the superiority of the replicon system compared to the T-DNA in plant GT, as the GT efficiencies were enhanced 5-8-fold with the replicons compared to that of the T-DNA tools (Fig. 2c and Supplemental Fig. 5).

Moreover, in keeping with our previous data[12], all of the LbCas12a-based GT constructs, except the 20-nt gRNA, exhibited significantly higher GT efficiencies than the SpCas9-based GT tools (Fig. 2c, 9.53 ± 0.53% of pHRC01 vs. 5.1 ± 0.34% of pHRC04, 9.53 ± 0.53% of pHRC03 vs. 6.73 ± 0.52% of pHRC05). These results also indicate that the 23-nt gRNA LbCas12a mediated GT more effectively than the 20-nt gRNA (pHRC03 vs. pHRC02). Surprisingly, analysis of the indel mutation efficiency of the guide RNAs at the plant stage demonstrated a reverse correlation between the indel mutation efficiency and the GT efficiency at cutting site 1 and cutting site 2 (Fig. 2d, pHRC01 vs. pHRC04 and pHRC03 vs. pHRC05, Supplemental Fig. 5). This result indicates that a considerably stronger indel mutation activity may negatively affect the GT reactions. Since cNHEJ-mediated indel mutations are favored throughout the life cycle of the cells and HDR is limited to the S-G2 phases[3], DNA DSBs that form at cell cycles other than S-G2 may lead to permanent modifications at the cutting sites, resulting in the inhibition of any further cleavage at these sites in the HDR-favorable cell cycles. Our data confirmed the stronger activity of SpCas9 in generating DNA DSBs compared to that of LbCas12a in tomato. The highest indel mutation rate was 49.5% on average with sgR2^{ANT1} (Supplemental Fig. 5). Most of the mutation

traces appear to be deletions (Supplemental Fig. 6). In the experiment, we obtained GT events with a typical purple phenotype due to the overexpression of SlANT1 and the subsequent accumulation of anthocyanin in the plants (Supplemental Fig. 7)

ttLbCas12a-based GT efficiency is higher than that of the wild-type variant in the case of the dual crRNA system.

The cleavage activity of Cas nucleases was shown to be temperature-dependent, especially in the case of LbCas12a[19]. Previously, we showed the temperature dependency of CRISPR/Cas-mediated GT in tomato[12]. In that case, LbCas12a exhibited considerably better GT support at temperatures as high as 31 °C compared to that at 19 °C or 25 °C. This result partially explained why SpCas9 was superior in indel mutation formation compared to LbCas12a at RT. Recently, Puchta's group reported a temperature-tolerant LbCas12a variant that significantly enhanced indel mutation[20] and GT[21, 29] efficacy in plants. It is interesting to characterize and compare the ttLbCas12a nuclease using our replicon system and on somatic cells of tomato. We investigated the impacts of single and dual cleavages using 20- or 23-nt gRNA on the GT performance of both the wild-type and ttLbCas12a variants at the well-characterized SlANT1 locus (Fig. 3a; Supplemental Fig. 4 and Data S1). To contribute to the comparison data, another dual crRNA (crR1-2.23^{ANT1}) was also tested with LbCas12a_gRNA2 (Supplemental Fig. 4), which was previously used by Vu and coworkers[12]. Our data collected from 6 biological replicates were processed and compared using uncorrected Fisher's LSD test. The statistical analysis demonstrated very mild GT efficiency changes among the GT constructs using single crRNAs with both LbCas12a variants (Fig. 3b; pHRC11, pHRC12 and pHRC13 for LbCas12a; and pHRC17, pHRC18 and pHRC19 for ttLbCas12a). There was no significant GT efficiency difference among

197 the single crRNAs or dual crRNAs with LbCas12a. However, the ttLbCas12a-based dual crRNA
198 constructs (pHRC20, pHRC11 and pHRC22) showed higher GT efficiencies than LbCas12a
199 (pHRC14, pHRC15 and pHRC16, respectively), although the p-values were close to 0.05 and
200 significant (Fig. 3b). The highest difference in GT efficiency was found between ttLbCas12a-
201 containing pHRC21 (9.74 ± 1.49%) and LbCas12a-containing pHRC15 (6.44 ± 0.75%) with crR1-
202 3.20^{ANT1}, exhibiting a 1.51-fold change (p = 0.07) (Fig. 3b, c).

203 In parallel with these experiment, we utilized targeted deep sequencing to analyze the cleavage
204 activity of the nucleases with each of the gRNAs (Fig. 3c) at 10 dpt. Due to the large size
205 (~0.3x0.3 cm) of the cotyledon explants used in the previous study, the majority of the cells
206 were not in direct contact with the agrobacteria and thus were not transformed efficiently.
207 Therefore, we reduced the size of the cotyledon explant to ~0.1x0.3 cm (Supplemental Fig. 8) to
208 assess the editing efficiency by targeted deep sequencing. The data collected from two
209 biological replicates showed strong enhancement of indel mutation efficiencies of a gRNA if it
210 was used in a dual crRNA construct, regardless of the LbCas12a variants. The largest
211 enhancement was from LbCas12a_gRNA1 (23 nt) in $crR1.23^{ANT1}$-carrying pHR11 (0.05%) and
212 crR1-3.23^{ANT1}-expressing pHRC16 (1.66%) in replicate 1, representing a 33.2-fold increase (Fig.
213 3c). The cleavage activity of ttLbCas12a was also higher than that of the WT variant when single
214 cuts were used. For example, in the case of the $crR1.23^{ANT1}$-expressing constructs, the indel
215 mutation efficiency was 5.00- to 7.29-fold increased with ttLbCas12a (pHRC17) compared to
216 LbCas12a (pHRC11) (Fig. 3c). For the cases of the dual crRNAs, ttLbCas12a showed more
217 balanced indel mutation efficiencies between the two gRNAs used in the same construct,
218 especially when dual crR1-3.20^{ANT1} with 20-nt gRNAs was examined (Fig. 3c, pHRC21 and

pHRC22 compared to pHRC15 and pHRC16, respectively). This activity might be one of the reasons that better enhancement of GT efficiency was mediated by ttLbCas12a compared to the WT version.

ttLbCas12a shows better performance than WT LbCas12a in allele-associated marker-free GT at the SlHKT1;2 and SlEPSPS1 loci

To further validate and utilize ttLbCas12a in our research on GT, we compared its performance at the two loci without using any donor-associated selection marker, and no allele-associated selection was employed during the experiments. The salt-tolerant allele SlHKT1;2 (N217D) (Fig. 4a) was successfully edited using our LbCas12a-based GT system[12], although at low efficiency. We introduced two glyphosate-resistant alleles of tomato 5-enolpyruvylshikimate-3-phosphate synthase 1 (SlEPSPS1): (1) T178I and P182S (TIPS allele, corresponding to T103I and P107S in maize, patent no. US6566587B1)[30] (Fig. 4b) and (2) G177A and A268T (GAAT allele, corresponding to G102A and A193T in maize, patent no. US 6225114 B1)[31] (Supplemental Fig. 9). Extensive comparisons of GT efficiency between LbCas12a and ttLbCas12a were conducted with single crRNAs (crR1.20$^{HKT1;2}$ and crR2.20$^{HKT1;2}$) and dual crRNAs (crR1-2.20$^{HKT1;2}$ and crR1-2.23$^{HKT1;2}$) (Fig. 4a; Supplemental Fig. 10 and Data S1) at the SlHKT1;2 locus. A T-DNA-based GT construct was also used in parallel with the replicon-based construct and the dual crR1-2.20$^{HKT1;2}$ construct. Additional comparisons were performed with the dual crRNAs crR1-2.23^{EPSPS1} and crR1-3.23^{EPSPS1} (Fig. 4b; Supplemental Fig. 10 and Data S1) to replace the TIPS and GAAT alleles, respectively, at the SlEPSPS1 locus.

GT efficiency was calculated by GT deep sequencing reads that only showed precise gene editing at both loci in cases of dual crRNAs, although at low efficiencies (Fig. 4c). No GT read

241 was obtained from the replicon-based single crRNA constructs and the T-DNA-based dual crRNA
242 regardless of the LbCas12a variants. At the SlHKT1;2 locus, the GT efficiency was higher for
243 ttLbCas12a using the dual 20-nt crRNA (crR1-2.20$^{HKT1;2}$), but contrasting results were obtained
244 with the longer dual crRNA (crR1-2.23$^{HKT1;2}$) (Fig. 4c). However, we obtained higher GT
245 efficiency with the 23-nt dual crRNA (crR1-2.23^{EPSPS1}) for the replacement of the TIPS allele
246 using ttLbCas12a (Fig. 4c). These data indicate that the targeted deep sequencing method may
247 help to identify the GT reads among the constructs, although the read numbers were still too
248 low to be used for statistical comparisons. The indel mutation efficiency obtained from the T-
249 DNA construct was up to 15-fold lower than that of the replicon using the same crR1-2.20$^{HKT1;2}$
250 (Fig. 4c). In this experiment, the indel mutation efficiencies of the single gRNAs were also lower
251 than those of the dual crRNAs. The highest indel mutation activity was obtained with crR1-
252 2.20$^{HKT1;2}$ and LbCas12a, yielding values of 4.32% of LbCas12a_gRNA1 and 2.56% of
253 LbCas12a_gRNA2. The gap between the indel mutation efficiencies of LbCas12a_gRNA1 and
254 LbCas12a_gRNA2 from crR1-2.20$^{HKT1;2}$ was also lower in the case of ttLbCas12a. However,
255 ttLbCas12a did not perform well when it was expressed with the 23-nt dual crRNA (crR1-
256 2.23$^{HKT1;2}$); hence, no GT read was obtained at 10 dpt using the combination (Fig. 4c). In general,
257 between the two replicates, higher indel activity in a construct was correlated with higher GT
258 efficiency.

259 Additional experiments for the exchange of the GAAT allele using the 23-nt dual crRNAs with
260 two (crR1-3.23^{EPSPS1}) or four cleavage sites (crR1-2.23^{EPSPS1} and crR2-4.23^{EPSPS1}) and the
261 LbCas12a variants (Supplemental Figs. 9-10) demonstrated that ttLbCas12a performed better in
262 either case. In triplicate, the highest GT efficiency was obtained with ttLbCas12a-expressing

263 constructs (pHRES2.11 compared to pHRES2.9) using the dual gRNA crR1-3.23^{EPSPS1}, up to 0.015
264 ± 0.015% for G177A and 0.018 ± 0.009% for A268T (Fig. 5a). Notably, the four gRNA constructs
265 (pHRES2.10 and pHRES2.12) showed a mild reduction in the gRNA1 and gRNA3 indel mutation
266 efficiencies, which were expected to be higher than those of the dual gRNA-expressing
267 constructs due to the synergistic effects of two close cleavage sites (Fig. 5a).

268 To further validate the performance of the LbCas12a variants, we screened and analyzed
269 transformants obtained from the transformation of the LbCas12a- and ttLbCas12a-based
270 constructs for the exchange of the TIPS allele. CAPS screening by BpiI digestion of the PCR
271 products flanking SlEPSPS1-targeted site 1 demonstrated potential TIPS allele-carrying events
272 (Fig. 5b). The BpiI site located 84 bp downstream of the T178 codon was modified during the
273 cloning of the homologous DNA donor through the Golden gate cloning method. Therefore, the
274 undigested bands that appeared on the agarose gel were potentially derived from the TIPS-
275 carrying alleles. Subsequent Sanger sequencing of the purified PCR products from 52
276 transformants per LbCas12a variant and analysis of their.ab1 files by ICE Synthego[32] identified
277 GT events carrying the TIPS allele (Supplemental Figs. 11-12) at various rates up to 17% (Fig. 5c,
278 left panel). The average GT efficiency obtained with ttLbCas12a (5.67 ± 0.74%) was slightly
279 lower than that of the WT version (4.69 ± 0.73%), although the difference was not significant.
280 The difference in plant stage GT efficiency is in contrast with the observation conducted
281 previously by targeted deep sequencing of the 10 dpt cotyledon samples (Fig. 4c). Nevertheless,
282 indel mutation efficiencies at the plant stage correlated with those obtained by targeted deep
283 sequencing (Fig. 5c, right panel). The average indel mutation efficiency was 34.52 ± 3.30% with
284 LbCas12a and lower for ttLbCas12a (26.94 ± 3.40%) ($p = 0.07$, Student's t-test). Notably, most of

the SlEPSPS1 TIPS allele-carrying GT plants showed no phenotypic changes (Supplemental Fig. 12). Several events that contained high indel mutation rates exhibited phenotypic defects compared to WT (Supplemental Fig. 12, pHRES2.7 events #27 and 28).

NU7441 treatment enhances the ttLbCas12a-base GT in tomato

Previously, NU7441 exhibited significant enhancement of LbCas12a-based GT (Fig. 1b). To further improve ttLbCas12a-based GT in tomato, we investigated the impacts of various NU7441 concentrations on the GT process using ttLbCas12a constructs with crR1-2.20^{HKT12}. Targeted deep sequencing data demonstrated the enhancement of GT efficiency with 1 µM NU7441 added to the culture medium. However, when the NU7441 concentrations were higher, the GT efficiency was lower than that of the mock control (Fig. 5d). Notably, the NU7441 treatments at various concentrations showed only mild changes in the indel mutation efficiency of gRNA1 and gRNA2 of the dual crRNA (Fig. 5d).

Discussion

The introduction of DNA DSB(s) at the targeted sites was shown to dramatically enhance GT efficiency in plants[6]. DSB repair is dictated by the NHEJ mechanism due to the abundance of KU70/80 and the other components in the cells[3]. Therefore, the plant HDR efficiency is considerably lower than that of NHEJ. The HDR pathway is more strictly dependent on the cell cycle, and even during favorable S-G2 phases, HDR must also compete with NHEJ to repair DNA DSBs. Previously, accumulated data in animal and plant studies showed the possibility of regulating repair pathway determination or inhibiting cNHEJ components by biochemical or chemical approaches[14, 16-18, 22, 23, 33, 34]. Among the chemicals that exhibited positive effects on

306 HDR or GT in animals, we chose to study several chemicals that inhibit the cNHEJ component(s)
307 to enhance GT efficiency in tomato.

308 DNA ligase IV was shown to be involved in the last step of cNHEJ-mediated DSB repair to seal
309 the broken ends of DNA DSBs. In a cell-free system, human DNA ligase IV was inhibited by SCR7,
310 a small molecule chemical, by blocking its DNA binding activity[34]. SCR7 at a concentration of 1
311 μM was shown to enhance CRISPR/Cas9-based GT efficiency up to 5-fold[22] or 19-fold[17] in
312 mammalian and mouse cells, and 10 μM or 60 μM SCR7 treatment led to reduced transfection
313 efficiency and cell viability. However, our data demonstrate only a moderate increase in GT
314 efficiency with the SpCas9 construct at toxic levels of SCR7 in animals and no significant
315 enhancement of GT efficiency in the case of LbCas12a (Fig. 1a). Because DNA ligase IV inhibition
316 by SCR7 was irrespective of the DSB configuration[34], the DNA DSBs generated by either SpCas9
317 or LbCas12a was not expected to affect the inhibition strength. Since our improved LbCas12a-
318 based GT system showed high efficiency under the experimental conditions, the addition of
319 SCR7, which affects the final step of cNHEJ, may not be recognized easily, and the impacts of its
320 toxicity level may be more visible (Fig. 1a). There were limited data regarding the uses of SCR7
321 for CRISPR/Cas-based GT enhancement in plants; therefore, it is unclear if the SCR7 treatment
322 is species-dependent, since the uptake of SCR7 may be different in plants. The enhancement
323 impacts of SCR7 were also controversial in animals, since studies that used human cell lines or
324 rabbit embryos did not show significant improvement of CRISPR/Cas9- or TALEN-based GT
325 efficiency by SCR7[18, 35, 36].

326 One of the alternative strategies for blocking the cNHEJ pathway is to inhibit the DNA-PKcs or
327 the other DNA-dependent protein kinases of the PI-3K family by NU7441[37] or KU0060648[38].

328 Studies conducted on mammalian cells showed that CRISPR/Cas9-based GT efficiency is
329 enhanced up to twofold by using NU7441 or KU0060648[16]. However, treatment with 1 μM
330 NU7441 and 200 nM KU0060648 did not significantly enhance the SpCas9-based GT efficiency
331 under our experimental conditions, although only NU7441 significantly enhanced the LbCas12a-
332 based GT efficiency up to 1.51-fold (Fig. 1b). Since no plant homologs of DNA-PKcs have been
333 identified, these data were surprising but were within our expectations for the existence of
334 other types of plant DNA-dependent protein kinases[3]. More importantly, these data indicate
335 that the inhibitory effects of NU7441 and KU0060648 were selective for the kinase forms and
336 the configurations of DNA DSB ends. Notably, although KU0060648 showed a wider range of
337 inhibition of both DNA-PKcs and PI-3K compared to NU7441, only NU7441 had a positive
338 impact on the LbCas12a GT tools, indicating that the DNA-PKcs targets of KU006648 and
339 NU7441 were distinct.

340 To further improve GT systems, recent studies using polyamines[24] and silver nitrate, a
341 polyamine biosynthesis regulator, were conducted. In a cell-free assay, polyamines were shown
342 to facilitate RAD51 activities during the formation of synaptic complexes and strand invasion.
343 Depletion of polyamines resulted in the impairment of HDR in mouse hair follicle cells.
344 However, to the best of our knowledge, no direct evidence of the addition of polyamines
345 exerting stimulatory effects on HDR has been reported. Although direct supplementation with
346 polyamines did not affect the CRISPR/Cas-based GT efficiency under our experimental
347 conditions, when we treated the explants with silver nitrate, indirect stimulation of polyamine
348 production using silver nitrate resulted in an increase in GT events, which appeared as purple
349 counting data (Supplemental Fig. 3a). Silver nitrate might also suppress the activities of

ethylene released under the stress induced by agrobacteria and tissue culture processes, leading to the promotion of embryogenic callus proliferation and subsequent somatic embryogenesis (Supplemental Fig. 3b).

Previously, we showed that our LbCas12a-based GT system mediated GT more effectively than did SpCas9 complexes[12]. However, direct evidence for the comparison are still required, considering that the accessibility of the cleavage sites and loci by CRISPR/Cas complexes may exhibit different results. Therefore, in this study, we selected the well-characterized SlANT1 locus and its two cleavage sites (1 and 3) to compare the two nucleases using the same or very closed gRNA binding sites (Fig. 2a and Supplemental Fig. 4). The only difference between the SpCas9- and LbCas12a-based vectors was the coding sequence of each of the nucleases, and they were both human-codon optimized (Fig. 2b and Data S1). As expected, the LbCas12-based GT tools outperformed the SpCas9-based replicons at the same cleavage sites (Fig. 2c). Notably, assessment of indel mutation efficiencies of the two systems at the plant stage demonstrated a reverse correlation with the GT efficiencies, as the SpCas9-based indel mutation efficiencies were significantly higher than those of the LbCas12a complexes at the tested cleavage sites (Fig. 2d and Supplemental Fig. 5). We reason that the strong cleavage activities of the SpCas9 complexes at all the cell cycles may lead to inhibition of the cleavage sites for further recurrent cuts and hence a reduction in the probability of homologous DNA donor-mediated repair by GT in the S-G2 HDR favorable phases. Another important point is that LbCas12a cleaves the targeted sites at a distal side of the TTTV PAM; hence, recurrent cleavages may be possible if the DSB repair of the first cut did not affect the seed sequence located at the proximal side of the PAM[12]. The view was also supported by a recent study[29]. We cannot exclude the possibility

372 that the difference in the DNA DSB configurations of SpCas9 (mostly blunt ends) and LbCas12a
373 (cohesive ends) differentially determined repair pathway activation in a spatiotemporal
374 manner, which resulted in the difference in GT efficacy of the two nucleases. In addition, this
375 experiment also indicates that the T-DNA-based gene editing efficiencies were notably low
376 compared to that of the replicon system (Fig. 2c, d) at the same cleavage sites due to its low
377 copy nature.

378 Recently, in attempts to further improve GT efficiency in plants, Puchta's group found that a
379 single mutation (D156R) of LbCas12a significantly improved GT performance compared to WT
380 nuclease[29, 39], especially at the optimal temperature for plant growth. However, a direct
381 comparison of the LbCas12a variants in somatic cell systems has not been reported. Our data
382 not only provide a direct comparison of the two nucleases but also showed their crRNA
383 preference (Fig. 3) in tomato somatic cells for practical applications. There was no significant
384 improvement in GT efficiency using single crRNAs, but ttLbCas12a-base GT might be enhanced
385 with the dual crRNAs, especially with the 20-nt gRNAs at the SlANT1 locus (Fig. 3c, d). The weak
386 improvement in GT efficiency mediated by ttLbCas12a could be explained by the high-
387 temperature experimental conditions applied from day 3 to day 12 throughout our study
388 (Supplemental Fig. 1), which might reduce the low temperature tolerance advantage of
389 ttLbCas12a. Further comparison of the LbCas12a variants at the other two loci, SlHKT1;2 and
390 SlEPSPS1, without using a donor or GT allele-associated selection marker showed better
391 performance of ttLbCas12a with dual 20-nt crRNAs at SlHKT12a (Fig. 4) and dual 23-nt crRNAs
392 at SlEPSPS1 loci (crR1-2.23^{EPSPS1} and crRNA1-3.23^{EPSPS1}) (Figs. 4 and 5a). The data demonstrated
393 the importance of using two neighboring (Fig. 4a, b) or distancing cleavages (Supplemental Fig.

9) for efficient GT, as this approach might offer synergistic effects in the case of neighboring cleavages that lead to considerably higher cutting[40]. In the case of GT alleles that require two distanced sequence modifications, such as the GAAT allele of the SlEPSPS1 loci, two DSBs flanking the targeted sites may ensure simultaneous exchanges of the sequences, since the HDR-based conversion tract generated from each targeted site may not cover the other, due to length limitations[29].

Analysis of the transformants obtained from the GT experiment for exchanging the TIPS allele of SlEPSPS1 revealed high GT efficiency at the plant stage (Fig. 5b, c), although no significant improvement in ttLbCas12a was found at this stage (Fig. 5c). GT events carrying up to 17% of the GT allele (Fig. 5c) were found with either abnormal or normal phenotypes compared to WT parental plants (Supplemental Fig. 12). The abnormality of the GT events, especially those obtained from the LbCas12a-based construct, was due to the high rates of SlEPSPS1 indel mutation alleles present in the same event. The malfunction of the SlEPSPS1 protein might lead to the inefficiency of aromatic amino acid biosynthesis, which causes phenotypic defects. In this regard, ttLbCas12a, which showed similar GT efficiency but a lower indel mutation rate, may be a better choice for plant GT. Finally, we confirmed the stimulating impacts of 1 μM NU7441 on ttLbCas12a-based GT performance, which may enhance the system further and facilitate practical applications for precision crop improvement.

Conclusion

The natural HDR efficiency in plant somatic cells is too low to be utilized for practical applications of GT-mediated plant breeding. Continuous efforts to improve GT performance

have been undertaken for precision crop breeding. In this study, we further improved the LbCas12a-based GT system with the use of chemical treatments (1 μM of NU7441 and/or AgNO3). The impacts of small molecule chemical treatments on GT have not been well studied in crop plants. Therefore, our data for the assessment of the effects of SCR7, NU7441, and KU0060648 treatments on GT efficiency may help to elucidate their impacts and possible targeted components for HDR pathway regulation in plants.

Our data show that LbCas12a outperformed SpCas9 under the same experimental conditions at the SlANT1 loci. Similar effects of the replicon system for GT are also clearly indicated. Despite the milder stimulatory effects on GT performance under our experimental conditions due to the high-temperature protocol, the results of this study indicate that ttLbCas12a might be a good choice for future applications in practical GT in plants. Taken together, the combination of the replicon with ttLbCas12a, double cleavages flanking the modification sequence, and the addition of NU7441 and/or AgNO3 and appropriate temperature conditions are important parameters for the application of GT in future practical applications in precision plant breeding.

Methods

System design for plant GT in tomato

The SlANT1, SlHKT1;2, and SlEPSPS1 loci were used to conduct HDR-based DNA insertion and allele replacement experiments. The chemical treatment experiments used a single replicon (pTC217 and pHR01) and multiple-replicon tool (pMR01) vectors from previous works[10, 12] to target the SlANT1 gene. The SpCas9 containing the pTC217 vector was ordered from Addgene (Plasmid #70018)[10]. Further works used the single replicon system as a vector for the delivery of

436 guide RNA and CRISPR/Cas expression cassettes and GT donor templates in this study (Figure 2a
437 and Data S1).

438 For comparison of the SpCas9 and LbCas12a complexes in GT performance, we designed an
439 HDR-mediated insertion of selection markers at the SlANT1 locus that was well studied in our
440 laboratory[12]. The gRNA binding and cutting sites were selected in a manner that could be used
441 for both SpCas9 (SpCas9_gRNA1 and SpCas9_gRNA2) and LbCas12a (LbCas12a_gRNA1 and
442 LbCas12a_gRNA3) (Figure 2a). We used a single gRNA for each of the GT vectors with either
443 SpCas9 or LbCas12a (Figure 2b). At the cutting site of LbCas12a_gRNA3, two different gRNA
444 lengths (20 and 23 nt) were tested (Figure 2b). All the editing constructs in the experiment were
445 delivered by *Agrobacterium*-mediated transformation of tomato cotyledon explants, and two
446 sets of constructs were cloned: one set with the single geminiviral replicon system[12] for the
447 amplification of homologous DNA donors and the other T-DNA set for comparison.

448 For the assessment and characterization of the activities of ttLbCas12a in GT in comparison
449 with the wild-type version of LbCas12a, similar constructs were designed for targeting the
450 SlANT1 locus with single LbCas12a gRNA expression cassettes. In addition, dual guide RNA
451 expression cassettes combining LbCas12a_gRNA1 (20 and 23 nt) and LbCas12a_gRNA3 (20 and
452 23 nt) were also used for the GT experiments (Figure 3a and Data S1).

453 A similar system for comparison of ttLbCas12a and wtLbCas12a was designed for targeting the
454 SlHKT1;2 and SlEPSPS1 loci (Fig. 4a, b). Single and dual cutting sites were used for SlHKT1;2
455 (Figure 4a, band Data S1). The gRNA lengths (20 and 23 nt) were also evaluated at the same

locus. For SlEPSPS1, only dual gRNAs 23 nt in length were assessed for GT with the LbCas12a variants (Figure 4a, b and Data S1).

In all the GT vectors, the expression of SpCas9 and LbCas12a variants was driven by a long CaMV 35S promoter that contains an intron (Trp1) at the 5'UTR. A copy of AtUBQ10 intron 1 was also inserted in the coding sequence of the LbCas12a variants (Data S1), which was tested previously for GT experiments by Vu and coworkers[12]. The crRNA and sgRNA expression cassettes were transcribed with the support of the core sequence of the AtU6 promoter[41].

Agrobacterium-mediated tomato transformation and chemical treatments

Agrobacterium-mediated tomato transformation was conducted following our protocol (Supplemental Figure 1) published previously by Vu and coworkers[12]. For the treatment of chemicals, the chemicals at the tested concentrations were added to the NSEL medium. The total treatment time was 5 days (day 3 to day 8 post transformation (dpt)). For targeted deep sequencing, cotyledon samples were collected at 10 dpt.

Assessment of GT efficiency

For assessment of the GT efficiency at SlANT1, purple spot counting was conducted at 21 dpt, and purple plants were recorded at the hardening stage. The GT efficiency reflected by the purple spot numbers was calculated with normalization to the SlANT1 overexpression tool that was transformed in parallel with the GT tool. The calculation method was previously explained by Vu and coworkers[12].

For assessment of the GT efficiency at the SlHKT1;2 and SlEPSPS1 loci, targeted deep sequencing was conducted with thin cotyledon explants collected at 10 dpt. Sanger sequencing was performed to screen and validate GT plants.

Targeted deep sequencing

Genomic DNAs were isolated from the cotyledon explants using the CTAB method. The MiSeq sequencing service (MiniSeq™ System, Illumina, USA) was used. MiSeq samples were prepared in three PCRs according to the manufacturer's guidelines with genomic DNAs as templates for the first PCR. The first and second PCRs used primers listed in Supplemental Table 1, whereas the third PCRs were performed with the manufacturer's primers to assign sample IDs. The first PCR primers were designed for binding to the upstream and downstream sequences from the homologous donor sequence junctions to avoid amplifying the donor DNA sequences. The second PCR primers were designed to amplify 150-180-bp flanking the targeted base changes at the targeted sites. High-fidelity DNA Taq polymerase (Phusion, NEB, USA) was used for PCR. The MiSeq raw data FASTQ files were analyzed by the Cas-Analyzer tool[42]. The indel analysis window was set to 5 bases, with a comparison range covering both read ends. The GT efficiency was assessed using the corresponding donor sequence as the input HDR donor sequence.

Statistical analysis

All comparison experiments were conducted with at least 3 replicates, and data were recorded by purple spot counting, targeted deep sequencing, and plant event screening. Some of the experiments using targeted deep sequencing were conducted in two replicates. The editing data, statistical analysis, and plots were further processed by the MS Excel and GraphPad Prism programs and explained in detail in the legends of figures and/or tables. Pairwise comparison

data were tested with Student's t-test with unequal variance and two-tailed parameters. Similar parameters were applied for multiple comparisons using Fisher's LSD test. A difference was considered to be significant when the statistical tests returned a p-value < 0.05.

Acknowledgment

We wish to thank Mrs. Ngan Nguyen Thi and Mrs. Jeong Se Jeong for providing valuable technical support to this study. This work was supported by the National Research Foundation of Korea (Grant NRF 2020R1I1A1A01072130, 2020M3A9I4038352, 2020R1A6A1A03044344) and the Program for New Plant Breeding Techniques (NBT, Grant PJ01478401), Rural Development Administration (RDA), Korea.

Contribution

T.V.V. and J.Y.K. conceived and designed the research. T.V.V., D.T.H.D., M.T.T., Y.W.S., and Y.J.S. conducted experiments. T.V.V., D.T.H.D., M.T.T. and J.Y.K. analyzed data. T.V.V. wrote the manuscript. T.V.V. and J.Y.K. finalized the manuscript. All authors read and approved the manuscript.

Competing interests

The authors declare no competing interests.

References

1. Paszkowski, J., Baur, M., Bogucki, A. & Potrykus, I. Gene targeting in plants. *EMBO J* **7**, 4021-4026 (1988).
2. Puchta, H. & Hohn, B. Green light for gene targeting in plants. *Proc Natl Acad Sci U S A* **102**, 11961-11962 (2005).

3. Van Vu, T. et al. Challenges and Perspectives in Homology-Directed Gene Targeting in Monocot Plants. *Rice (N Y)* **12**, 95 (2019).
4. Terada, R., Urawa, H., Inagaki, Y., Tsugane, K. & Iida, S. Efficient gene targeting by homologous recombination in rice. *Nat Biotechnol* **20**, 1030-1034 (2002).
5. Puchta, H., Dujon, B. & Hohn, B. Homologous recombination in plant cells is enhanced by in vivo induction of double strand breaks into DNA by a site-specific endonuclease. *Nucleic Acids Research* **21**, 5034-5040 (1993).
6. Puchta, H., Dujon, B. & Hohn, B. Two different but related mechanisms are used in plants for the repair of genomic double-strand breaks by homologous recombination. **93**, 5055-5060 (1996).
7. Zhang, Y. et al. Transcription activator-like effector nucleases enable efficient plant genome engineering. *Plant Physiol* **161**, 20-27 (2013).
8. Shan, Q. et al. Targeted genome modification of crop plants using a CRISPR-Cas system. *Nat Biotechnol* **31**, 686-688 (2013).
9. Wright, D.A. et al. High-frequency homologous recombination in plants mediated by zinc-finger nucleases. *Plant J* **44**, 693-705 (2005).
10. Cermak, T., Baltes, N.J., Cegan, R., Zhang, Y. & Voytas, D.F. High-frequency, precise modification of the tomato genome. *Genome Biol* **16**, 232 (2015).
11. Gil-Humanes, J. et al. High-efficiency gene targeting in hexaploid wheat using DNA replicons and CRISPR/Cas9. *Plant J* **89**, 1251-1262 (2017).
12. Vu, T.V. et al. Highly efficient homology-directed repair using CRISPR/Cpf1-geminiviral replicon in tomato. *Plant Biotechnol J* (2020).
13. Butler, N.M., Baltes, N.J., Voytas, D.F. & Douches, D.S. Geminivirus-Mediated Genome Editing in Potato (Solanum tuberosum L.) Using Sequence-Specific Nucleases. *Front Plant Sci* **7**, 1045 (2016).
14. Endo, M., Mikami, M. & Toki, S. Biallelic Gene Targeting in Rice. *Plant Physiol* **170**, 667-677 (2016).
15. Qi, Y. et al. Increasing frequencies of site-specific mutagenesis and gene targeting in Arabidopsis by manipulating DNA repair pathways. *Genome Res* **23**, 547-554 (2013).

16. Robert, F., Barbeau, M., Ethier, S., Dostie, J. & Pelletier, J. Pharmacological inhibition of DNA-PK stimulates Cas9-mediated genome editing. *Genome Med* **7**, 93 (2015).
17. Maruyama, T. et al. Increasing the efficiency of precise genome editing with CRISPR-Cas9 by inhibition of nonhomologous end joining. *Nat Biotechnol* **33**, 538-542 (2015).
18. Song, J. et al. RS-1 enhances CRISPR/Cas9- and TALEN-mediated knock-in efficiency. *Nat Commun* **7**, 10548 (2016).
19. Malzahn, A.A. et al. Application of CRISPR-Cas12a temperature sensitivity for improved genome editing in rice, maize, and Arabidopsis. *BMC Biol* **17**, 9 (2019).
20. Schindele, P. & Puchta, H. Engineering CRISPR/LbCas12a for highly efficient, temperature-tolerant plant gene editing. *Plant Biotechnol J* **18**, 1118-1120 (2020).
21. Merker, L., Schindele, P., Huang, T.K., Wolter, F. & Puchta, H. Enhancing in planta gene targeting efficiencies in Arabidopsis using temperature-tolerant CRISPR/LbCas12a. *Plant Biotechnol J* **18**, 2382-2384 (2020).
22. Chu, V.T. et al. Increasing the efficiency of homology-directed repair for CRISPR-Cas9-induced precise gene editing in mammalian cells. *Nat Biotechnol* **33**, 543-548 (2015).
23. Zhang, J.P. et al. Efficient precise knockin with a double cut HDR donor after CRISPR/Cas9-mediated double-stranded DNA cleavage. *Genome Biol* **18**, 35 (2017).
24. Lee, C.Y. et al. Promotion of homology-directed DNA repair by polyamines. *Nat Commun* **10**, 65 (2019).
25. Beyer, E.M. A potent inhibitor of ethylene action in plants. *Plant Physiol* **58**, 268-271 (1976).
26. Giridhar, P., Indu, E.P., Vinod, K., Chandrashekar, A. & Ravishankar, G.A. Direct somatic embryogenesis from Coffea arabica L. and Coffea canephora P ex Fr. under the influence of ethylene action inhibitor-silver nitrate. *Acta Physiologiae Plantarum* **26**, 299-305 (2004).
27. Roustan, J.-P., Latche, A. & Fallot, J. Control of carrot somatic embryogenesis by AgNO3, an inhibitor of ethylene action: Effect on arginine decarboxylase activity. *Plant Science* **67**, 89-95 (1990).

28. Hanfrey, C., Sommer, S., Mayer, M.J., Burtin, D. & Michael, A.J. Arabidopsis polyamine biosynthesis: absence of ornithine decarboxylase and the mechanism of arginine decarboxylase activity. *Plant J* **27**, 551-560 (2001).
29. Huang, T.-K., Armstrong, B., Schindele, P. & Puchta, H. Efficient gene targeting in Nicotiana tabacum using CRISPR/SaCas9 and temperature tolerant LbCas12a. *Plant Biotechnol J* **doi:** https://doi.org/10.1111/pbi.13546 (2021).
30. Lebrun, M., Sailland, A., Freyssinet, G., DeGryse, E. Mutated 5-enolpyruvylshikimate-3-phosphate synthase, gene coding for said protein and transformed plants containing said gene. *US Patent no. US6566587B1* (2003).
31. Eichholtz, D.A., Scott, G.C., Murthy, K.G. Modified gene encoding glyphosate-tolerant 5-enolpruvyl-3-phosphoshikimate synthase. *US Patent no. US6,225,114B1* (2001).
32. Hsiau, T. et al. Inference of CRISPR Edits from Sanger Trace Data. 251082 (2019).
33. Nishizawa-Yokoi, A. et al. A Defect in DNA Ligase4 Enhances the Frequency of TALEN-Mediated Targeted Mutagenesis in Rice. *Plant Physiol* **170**, 653-666 (2016).
34. Srivastava, M. et al. An inhibitor of nonhomologous end-joining abrogates double-strand break repair and impedes cancer progression. *Cell* **151**, 1474-1487 (2012).
35. Gutschner, T., Haemmerle, M., Genovese, G., Draetta, G.F. & Chin, L. Post-translational Regulation of Cas9 during G1 Enhances Homology-Directed Repair. *Cell Rep* **14**, 1555-1566 (2016).
36. Yang, D. et al. Enrichment of G2/M cell cycle phase in human pluripotent stem cells enhances HDR-mediated gene repair with customizable endonucleases. *Scientific Reports* **6**, 21264 (2016).
37. Leahy, J.J. et al. Identification of a highly potent and selective DNA-dependent protein kinase (DNA-PK) inhibitor (NU7441) by screening of chromenone libraries. *Bioorg Med Chem Lett* **14**, 6083-6087 (2004).
38. Munck, J.M. et al. Chemosensitization of cancer cells by KU-0060648, a dual inhibitor of DNA-PK and PI-3K. *Mol Cancer Ther* **11**, 1789-1798 (2012).
39. Merker, L., Schindele, P. & Puchta, H. Using CRISPR/ttLbCas12a for in planta Gene Targeting in A. thaliana. *Curr Protoc Plant Biol* **5**, e20117 (2020).

604 40. Chen, F. et al. Targeted activation of diverse CRISPR-Cas systems for mammalian
605 genome editing via proximal CRISPR targeting. *Nat Commun* **8**, 14958 (2017).
606 41. Nekrasov, V., Staskawicz, B., Weigel, D., Jones, J.D. & Kamoun, S. Targeted mutagenesis
607 in the model plant Nicotiana benthamiana using Cas9 RNA-guided endonuclease. *Nat*
608 *Biotechnol* **31**, 691-693 (2013).
609 42. Park, J., Lim, K., Kim, J.-S. & Bae, S. Cas-analyzer: an online tool for assessing genome
610 editing results using NGS data. *Bioinformatics* **33**, 286-288 (2016).

611 Figure legends

612 **Fig. 1 Enhancement of GT efficiency by chemical treatments for blocking cNHEJ. a**. SpCas9
613 (pTC217, top panel) and LbCas12a (pHR01, bottom panel)-based GT efficiency obtained from
614 the treatment of different SCR7 concentrations. SCR7 was added to the nonselection medium
615 (NSEL), and the explants were incubated for 5 days before transferring to the selection medium
616 (SEL5). The GT efficiencies were calculated at 21 dpt. **b**. The impacts of KU0060648 and NU7441
617 on CRISPR/Cas-based GT. SpCas9-based pTC217 (top panel) and LbCas12a-based pHR01 (middle
618 panel) were cloned with single geminiviral replicons, whereas LbCas12a-based pMR01 (bottom
619 panel) was released from a multireplicon vector. The chemical was added to the nonselection
620 medium (NSEL), and the explants were incubated for 5 days before transferring to the selection
621 medium (SEL5). The GT efficiencies were calculated at 21 dpt. Multiple comparisons of the
622 means and plotting were conducted by GraphPad Prism version 9 using one-way ANOVA and
623 Fisher's LSD test. The p-values of each compared mean pair are shown on the top of the bars.

624 **Fig. 2 Performance of the LbCas12a and SpCas9 nucleases in GT-mediated DNA insertion in**
625 **tomato. a**. Schematic diagram of CRISPR/Cas-based GT processes. The SlANT1 genomic site was
626 cleaved by the CRISPR/Cas complexes at the positions of LbCas12a_gRNA1 and 3 and

SpCas9_gRNA1 and 2, denoted by scissors. Subsequent repairs of the DSBs were conducted with the addition of donor templates that contain upstream homologous arms (corresponding to Donor 3.up and Donor 4.up) and downstream truncated SlANT1 (corresponding to Donors 3 and 4.down) of the DSB sites and the inserted sequences containing the kanamycin selection marker (pNOS-NptII-tOCS) followed by a CaMV 35S promoter (35S) for constitutively driving SlANT1 expression. The lengths in bp of the homologous arms are also shown. The distances in bp among the cleaved sites and the starts and ends of the donor sequences were calculated and illustrated in relation to the ATG start codon of the SlANT1 gene with the A as the +1 position. The sequence upstream of the SlANT1 start codon is drawn by the green lines, and purple lines are drawn for the downstream part. The crossing discontinuous lines between the homologous DNA donor and genomic site depict the expected homologous recombination for sequence exchanges. Successful GT would integrate the selection marker and 35S promoter at the DSB sites, thereby supporting event selection and screening by kanamycin antibiotic and purple phenotype. **b**. Binary vectors used for comparison of SpCas9- and LbCas12a-based GT performance. Each vector contained a homologous donor described in (A) and Data S1, an expression cassette of sgRNA/crRNA and SpCas9 or LbCas12a expression cassette. Two sets of vectors were used: only T-DNA and replicon-based systems for comparison. **c**. Scatter dot-bar plots showing the GT efficiencies of the tested constructs. **d**, Boxplot showing the indel mutation efficiencies of the GT constructs at the plant stage. The GT efficiencies were calculated at 21 dpt. Multiple comparisons of the means and plotting were conducted by GraphPad Prism version 9 using one-way ANOVA and Fisher's LSD test. The p-values of each compared mean pair are shown on the top of the bars.

Fig. 3 Comparison of GT efficiency between LbCas12a and ttLbCas12a at the SlANT1 locus. a, Binary constructs with the same crRNAs and donors for the assessment of the GT efficiency of LbCas12a (left panel) and ttLbCas12a (right panel). **b**. Boxplot showing the distributions of GT efficiency among the tools using various crRNAs with LbCas12a and ttLbCas12a. Multiple comparisons of the means of GT efficiency of the constructs using the same sets of crRNAs and donors but with LbCas12a or ttLbCas12a were conducted using Fisher's LSD test, and the p-values are shown above the compared boxes. **c**, Indel mutation rates induced by the Cas-crRNA complexes that were assessed at 10 dpt by targeted deep sequencing method. The GT efficiencies are also added for comparison.

Fig. 4 GT performance of the LbCas12a variants at the SlHKT1;2 and SlEPSPS1 loci.

a-b. Schematic diagrams describing the expected GT processes for exchanging the homologous DNA donor template with the genomic sequence at the SlHKT1;2 (**a**) and SlEPSPS1 (**b**) loci. The D217 coding sequence was added during the cloning of the HKTD1 donor for exchange with the N217 sequence of the genomic site. The lengths of homologous arms are shown. Two cutting sites (LbCas12a cutting sites 1 and 2) were planned to support the GT. The reverse and forward primers for amplifying the targeted sites by PCR are shown with black arrows. The I178 and S182 coding sequences were added during the cloning of the EPSPS1D3 donor for exchange with the T178 and P182 sequences of the genomic site. The lengths of homologous arms are shown. Two cutting sites (LbCas12a cutting sites 1 and 2) were used for the GT experiments. The reverse and forward primers for amplifying the targeted sites by PCR are shown with black arrows. In **b**, LbCas12a cutting site 2 is set as position 1, and the other positions are calculated accordingly. The diagrams were drawn not to their actual scales. **c.** The GT and indel mutation

efficiencies assessed by targeted deep sequencing. At the SlHKT1;2 locus, four different crRNAs (single gRNAs: crR1.20^{HKT12}; crR2.20^{HKT12}, and dual gRNAs: crR1-2.20^{HKT12}; crR1.23^{HKT12}) were used for comparison of the LbCas12a variants in GT performance. A T-DNA vector was also used for comparison with the replicon system. With the SlEPSPS1 gene, only one dual gRNA construct (crR1-2.23^{EPSPS1}) was used with the two LbCas12a variants. Wt: wild-type LbCas12a; tt: ttLbCas12a.

Fig. 5 Further assessment of GT performance of the LbCas12a variants at the SlEPSPS1 locus. **a.** Assessment of GT efficiency by targeted deep sequencing with GT tools using two or four cutting sites with LbCas12a variants at the SlEPSPS1 locus. **b-c**. Indel mutation and GT efficiencies obtained with the LbCas12a variants at the plant stage. Fifty-two plants of each LbCas12a variant were obtained from the transformation of the GT tool with the crR1-2.23^{EPSPS1} expression cassette and used for PCR amplification of the targeted site with the UPEPSPS1-F2 and DNEPSPS1-R1 primers. In **b**, the PCR products were purified and screened for the potential GT allele by BpiI digestion since the BpiI site near the targeted site was modified in the DNA donor sequence. The red arrows indicate potential GT bands. 1-15: Representative transformants obtained from the transformation using the GT construct containing LbCas12a and crR1-3.23^{EPSPS1}. In **c**: All the purified PCR products were sequenced by the Sanger method, and the ab1 files were subsequently analyzed by ICE Synthego software to reveal the indel mutation and GT efficiencies. The indel mutation and GT efficiencies of all the samples were statistically analyzed using Student's t-test and plotted by GraphPad Prism version 9. The editing efficiencies (mean ± SEM) are shown at the bottom of each box. **d**. Targeted deep sequencing-mediated evaluation of NU7441 impacts on ttLbCas12a-based GT efficiency.

Supplemental Figure legends

Supplemental Fig. 1 *Agrobacterium*-mediated transformation protocol used in this work.

Supplemental Fig. 2 Effects of polyamine treatment on the GT efficiency.

Supplemental Fig. 3 Effects of AgNO3 treatment on purple spot numbers and purple shoot regeneration.

Supplemental Fig. 4 Map of SpCas9 and LbCas12a binding sites at the SlANT1 locus.

Supplemental Fig. 5 Editing performance of the T-DNA and replicon-based SpCas9 and LbCas12a GT tools at various sites of the SlANT1 locus.

Supplemental Fig. 6 Representative indel mutation traces of the GT constructs revealed from ICE Synthego analysis.

Supplemental Fig. 7 Representative SlANT1 GT events obtained from the study.

Supplemental Fig. 8 Thin slice cotyledon explants for the assessment of editing efficiencies by targeted deep sequencing at 10 dpt.

Supplemental Fig. 9 Diagram showing the strategy for replacement of two amino acids of the SlEPSPS1 gene.

Supplemental Fig. 10 GT constructs for editing the SlHKT1;2 and SlEPSPS1.

Supplemental Fig. 11 Representative of the TIPS allele revealed at the plant stage.

Supplemental Fig. 12 Representative GT events obtained using the GT tool for TIPS allele replacement.

Supplemental Tables

Supplemental Table 1. Sequences and primers used in this study.

Supplemental Table 2. Impacts of SCR7 on GT efficiency.

Supplemental Table 3. GT efficiency obtained from the treatment of RS1 and SCR7.

Supplemental Table 4. GT performance revealed from the treatment of KU0060648 and NU7441.

Supplemental Table 5. Shoot regeneration after treatment with KU0060648 and NU7441.

Supplemental Table 6. Negative impacts of ABA treatment on GT efficiency.

Supplemental Table 7. GT efficiency obtained from polyamine treatment.

Supplemental Table 8. GT efficiency of the AgNO3 and mock treatments of pMR01.

Figure 1

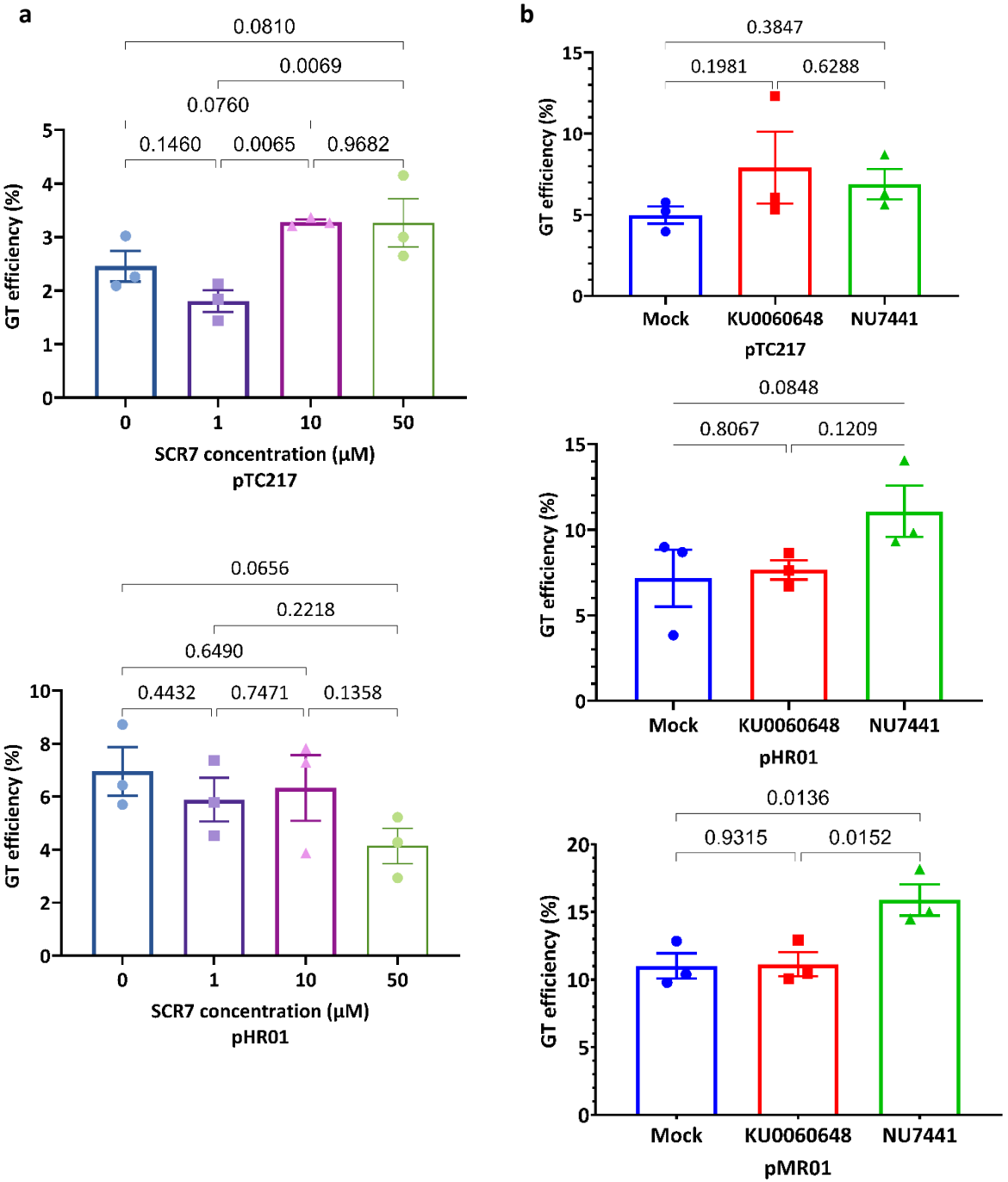
a
0.0810
0.0069
0.0760
0.1460
0.0065
0.9682
GT efficiency (%)
SCR7 concentration (μM)
pTC217
0.0656
0.2218
0.6490
0.4432
0.7471
0.1358
GT efficiency (%)
SCR7 concentration (μM)
pHR01
b
0.3847
0.1981
0.6288
GT efficiency (%)
Mock
KU0060648
NU7441
pTC217
0.0848
0.8067
0.1209
GT efficiency (%)
Mock
KU0060648
NU7441
pHR01
0.0136
0.9315
0.0152
GT efficiency (%)
Mock
KU0060648
NU7441
pMR01

Fig. 1 Enhancement of GT efficiency by chemical treatments for blocking cNHEJ. a. SpCas9 (pTC217, top panel) and LbCas12a (pHR01, bottom panel)-based GT efficiency obtained from the treatment of different SCR7 concentrations. SCR7 was added to the nonselection medium (NSEL), and the explants were incubated for 5 days before transferring to the selection medium (SEL5). The GT efficiencies were calculated at 21 dpt. **b**. The impacts of KU0060648 and NU7441 on CRISPR/Cas-based GT. SpCas9-based pTC217 (top panel) and LbCas12a-based pHR01 (middle panel) were cloned with single geminiviral replicons, whereas LbCas12a-based pMR01 (bottom panel) was released from a multireplicon vector. The chemical was added to the nonselection medium (NSEL), and the explants were incubated for 5 days before transferring to the selection medium (SEL5). The GT efficiencies were calculated at 21 dpt. Multiple comparisons of the means and plotting were conducted by GraphPad Prism version 9 using one-way ANOVA and Fisher's LSD test. The p-values of each compared mean pair are shown on the top of the bars.

Figure 2

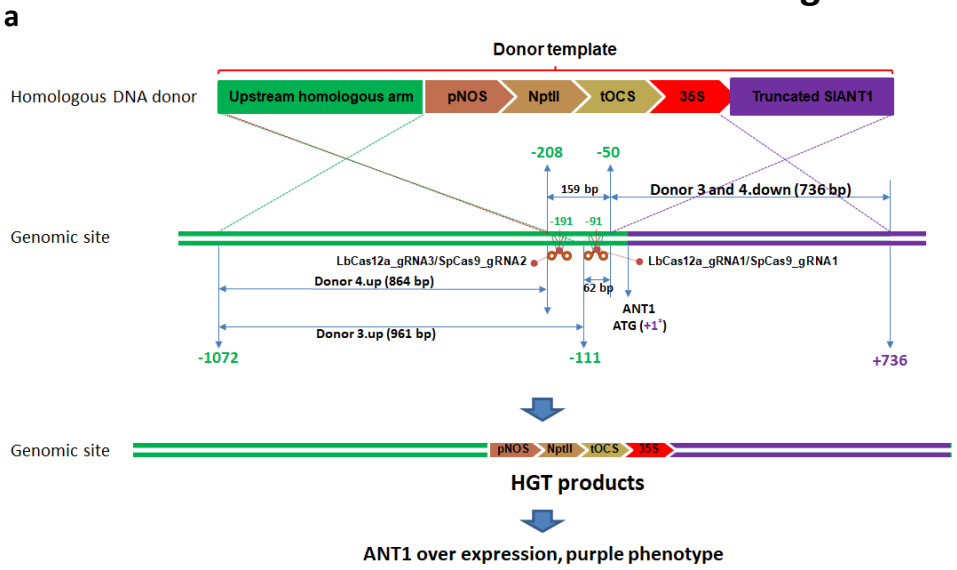
a
Donor template
Homologous DNA donor
Upstream homologous arm
pNOS
NptII
tOCS
35S
Truncated SlANT1
-208
-50
159 bp
Donor 3 and 4.down (736 bp)
Genomic site
-191
-91
LbCas12a_gRNA3/SpCas9_gRNA2
LbCas12a_gRNA1/SpCas9_gRNA1
Donor 4.up (864 bp)
62 bp
ANT1
ATG (+1)
Donor 3.up (961 bp)
-1072
-111
+736
Genomic site
HGT products
ANT1 over expression, purple phenotype

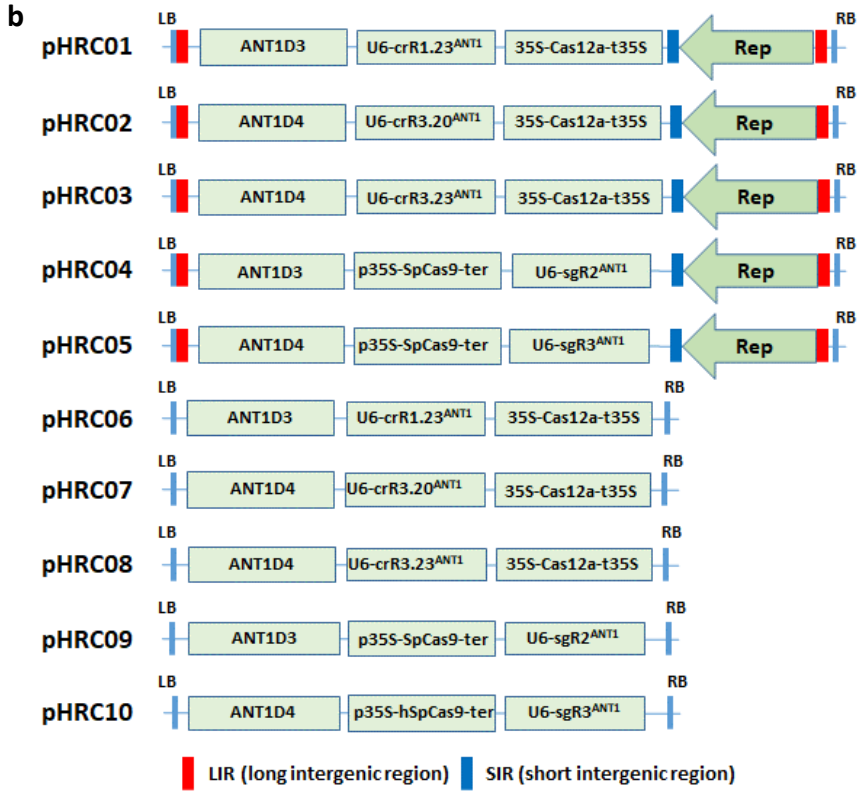
b
pHRC01
ANT1D3
U6-crR1.23ANT1
35S-Cas12a-t35S
Rep
pHRC02
ANT1D4
U6-crR3.20ANT1
35S-Cas12a-t35S
Rep
pHRC03
ANT1D4
U6-crR3.23ANT1
35S-Cas12a-t35S
Rep
pHRC04
ANT1D3
p35S-SpCas9-ter
U6-sgR2ANT1
Rep
pHRC05
ANT1D4
p35S-SpCas9-ter
U6-sgR3ANT1
Rep
pHRC06
ANT1D3
U6-crR1.23ANT1
35S-Cas12a-t35S
pHRC07
ANT1D4
U6-crR3.20ANT1
35S-Cas12a-t35S
pHRC08
ANT1D4
U6-crR3.23ANT1
35S-Cas12a-t35S
pHRC09
ANT1D3
p35S-SpCas9-ter
U6-sgR2ANT1
pHRC10
ANT1D4
p35S-hSpCas9-ter
U6-sgR3ANT1
LB
RB
LIR (long intergenic region)
SIR (short intergenic region)

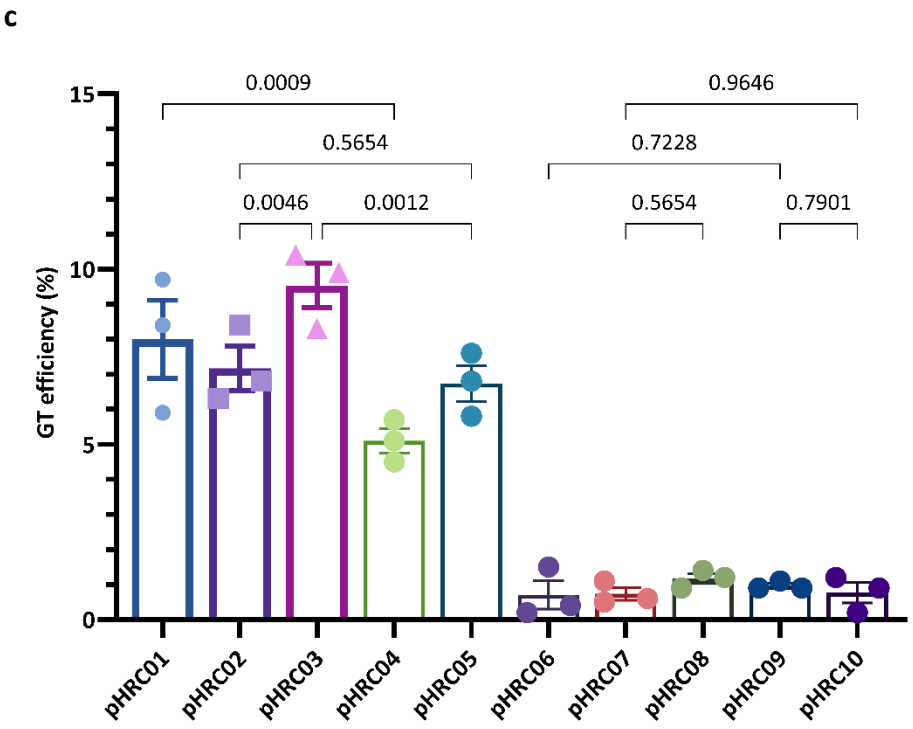
c
GT efficiency (%)
0.0009
0.9646
0.5654
0.7228
0.0046
0.0012
0.5654
0.7901
pHRC01
pHRC02
pHRC03
pHRC04
pHRC05
pHRC06
pHRC07
pHRC08
pHRC09
pHRC10

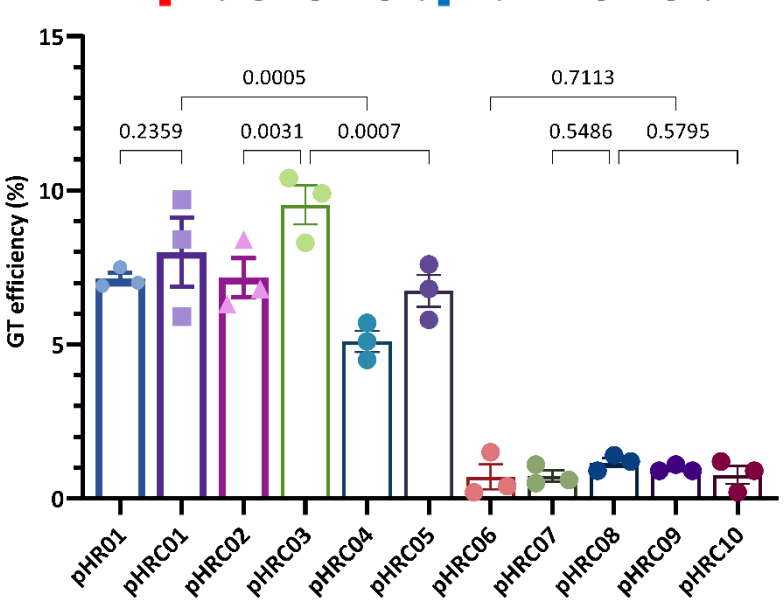
d
GT efficiency (%)
0.0005
0.7113
0.2359
0.0031
0.0007
0.5486
0.5795
pHR01
pHRC01
pHRC02
pHRC03
pHRC04
pHRC05
pHRC06
pHRC07
pHRC08
pHRC09
pHRC10

Fig. 2 Performance of the LbCas12a and SpCas9 nucleases in GT-mediated DNA insertion in tomato. a. Schematic diagram of CRISPR/Cas-based GT processes. The SlANT1 genomic site was cleaved by the CRISPR/Cas complexes at the positions of LbCas12a_gRNA1 and 3 and SpCas9_gRNA1 and 2, denoted by scissors. Subsequent repairs of the DSBs were conducted with the addition of donor templates that contain upstream homologous arms (corresponding to Donor 3.up and Donor 4.up) and downstream truncated SlANT1 (corresponding to Donors 3 and 4.down) of the DSB sites and the inserted sequences containing the kanamycin selection marker (pNOS-NptII-tOCS) followed by a CaMV 35S promoter (35S) for constitutively driving SlANT1 expression. The lengths in bp of the homologous arms are also shown. The distances in bp among the cleaved sites and the starts and ends of the donor sequences were calculated and illustrated in relation to the ATG start codon of the SlANT1 gene with the A as the +1 position. The sequence upstream of the SlANT1 start codon is drawn by the green lines, and purple lines are drawn for the downstream part. The crossing discontinuous lines between the homologous DNA donor and genomic site depict the expected homologous recombination for sequence exchanges. Successful GT would integrate the selection marker and 35S promoter at the DSB sites, thereby supporting event selection and screening by kanamycin antibiotic and purple phenotype. **b**. Binary vectors used for comparison of SpCas9- and LbCas12a-based GT performance. Each vector contained a homologous donor described in (A) and Data S1, an expression cassette of sgRNA/crRNA and SpCas9 or LbCas12a expression cassette. Two sets of vectors were used: only T-DNA and replicon-based systems for comparison. **c**. Scatter dot-bar plots showing the GT efficiencies of the tested constructs. **d**, Boxplot showing the indel mutation efficiencies of the GT constructs at the plant stage. The GT efficiencies were calculated at 21 dpt. Multiple comparisons of the means and plotting were conducted by GraphPad Prism version 9 using one-way ANOVA and Fisher's LSD test. The p-values of each compared mean pair are shown on the top of the bars.

Figure 3

a

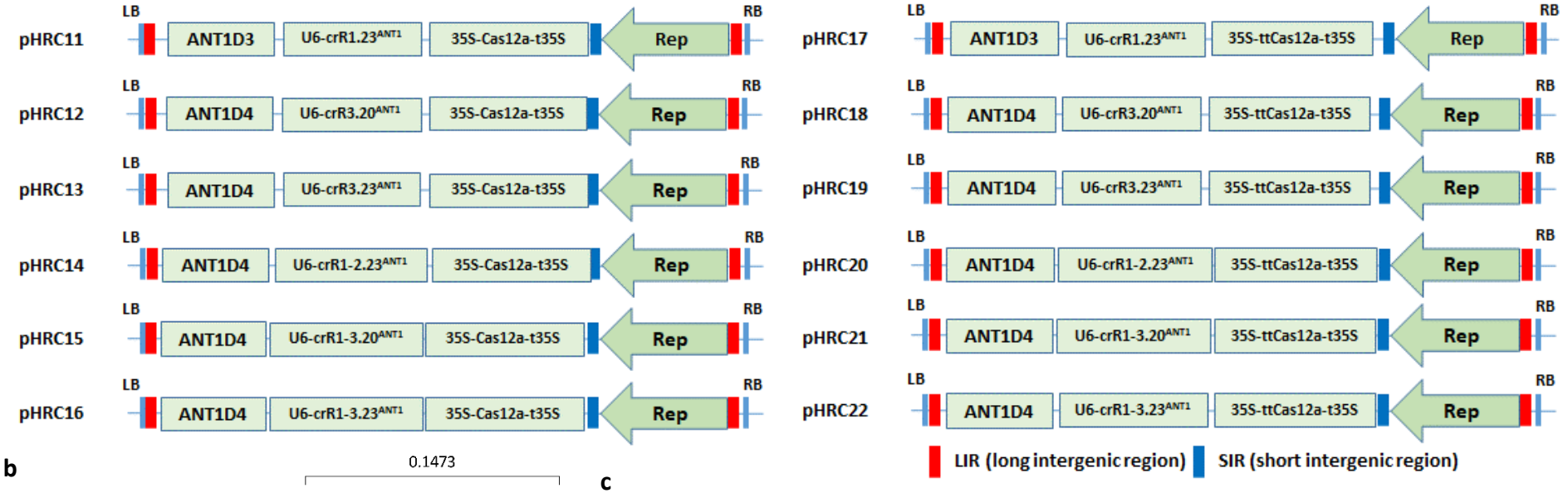

b

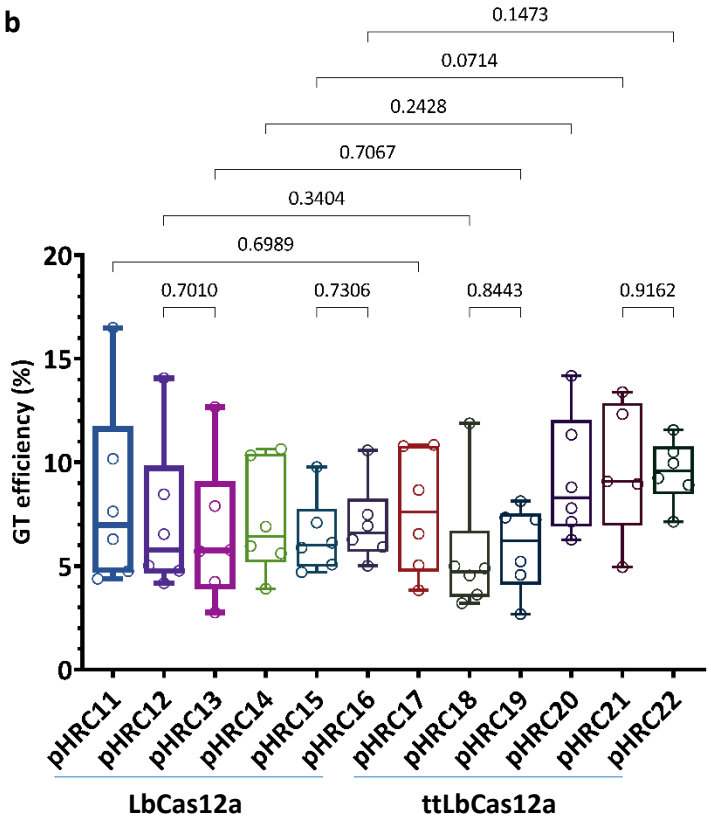

c

Construct	LbCas12a variant	ANT1 crRNA	Rep1			Rep2			GT efficiency (%)
			gRNA1 Miniseq indel rates (%)	gRNA2 Miniseq indel rates (%)	gRNA3 Miniseq indel rates (%)	gRNA1 Miniseq indel rates (%)	gRNA2 Miniseq indel rates (%)	gRNA3 Miniseq indel rates (%)	
pHRC11	wt	crR1.23	0.05	-	-	0.17	-	-	8.29±1.85
pHRC12		crR3.20	-	-	0.26	-	-	0.74	7.17±1.52
pHRC13		crR3.23	-	-	0.05	-	-	0.24	6.51±1.42
pHRC14		crR1-2.23	0.71	0.04	-	1.52	0.10	-	7.23±1.12
pHRC15		crR1-3.20	1.44	-	0.84	1.91	-	1.00	6.44±0.75
pHRC16		crR1-3.23	1.66	-	0.35	2.04	-	0.44	7.03±0.79
pHRC17	tt	crR1.23	0.20	-	-	1.24	-	-	7.62±1.21
pHRC18		crR3.20	-	-	0.12	-	-	1.52	5.52±1.31
pHRC19		crR3.23	-	-	0.14	-	-	0.85	5.86±0.84
pHRC20		crR1-2.23	0.36	0.05	-	0.83	0.12	-	9.25±1.21
pHRC21		crR1-3.20	1.34	-	1.49	1.60	-	1.62	9.74±1.49
pHRC22		crR1-3.23	1.72	-	1.00	3.00	-	2.31	9.55±0.62

Fig. 3 Comparison of GT efficiency between LbCas12a and ttLbCas12a at the SlANT1 locus. a, Binary constructs with the same crRNAs and donors for the assessment of the GT efficiency of LbCas12a (left panel) and ttLbCas12a (right panel). **b**. Boxplot showing the distributions of GT efficiency among the tools using various crRNAs with LbCas12a and ttLbCas12a. Multiple comparisons of the means of GT efficiency of the constructs using the same sets of crRNAs and donors but with LbCas12a or ttLbCas12a were conducted using Fisher's LSD test, and the p-values are shown above the compared boxes. **c**, Indel mutation rates induced by the Cas-crRNA complexes that were assessed at 10 dpt by targeted deep sequencing method. The GT efficiencies are also added for comparison.

Figure 4

a

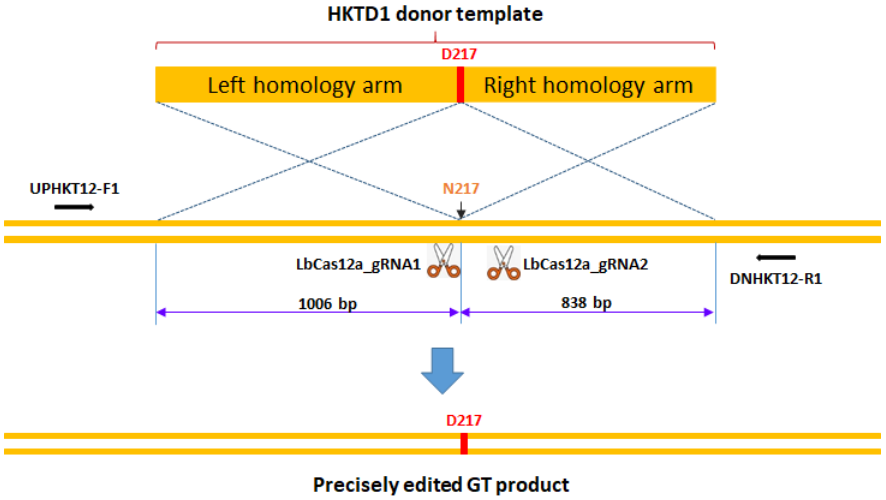

b

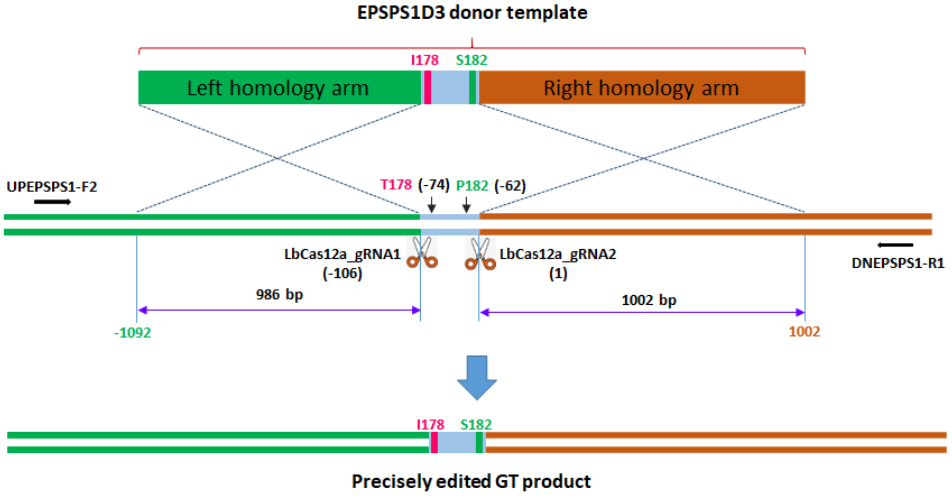

c

Targeted gene	Cargo	LbCas12a variant	crRNA	Replicate 1				Replicate 2			
				Total read	GT efficiency (%)	Indel rate of gRNA1 (%)	Indel rate of gRNA2 (%)	Total read	GT efficiency (%)	Indel rate of gRNA1 (%)	Indel rate of gRNA2 (%)
SlHKT1;2	Replicon	wt	crR1.20$^{HKT1;2}$	71070	0.000	0.74	-	46888	0.000	2.52	-
	Replicon	wt	crR2.20$^{HKT1;2}$	51658	0.000	-	0.24	49471	0.000	-	1.51
	T-DNA	wt	crR1-2.20$^{HKT1;2}$	58514	0.000	0.09	0.04	51889	0.000	0.52	0.17
	Replicon	wt	crR1-2.20$^{HKT1;2}$	46531	0.000	0.69	0.35	50341	0.002	4.32	2.56
	Replicon	tt	crR1-2.20$^{HKT1;2}$	43205	0.000	0.90	0.67	44029	0.005	3.87	2.39
	Replicon	wt	crR1-2.23$^{HKT1;2}$	26965	0.004	3.30	1.06	33146	0.010	2.91	0.62
	Replicon	tt	crR1-2.23$^{HKT1;2}$	20319	0.000	1.72	0.90	43393	0.000	1.49	0.71
SlEPSPS1	Replicon	wt	crR1-2.23^{EPSPS1}	59007	0.003	0.31	-	72638	0.006	1.89	-
	Replicon	tt	crR1-2.23^{EPSPS1}	40357	0.005	0.14	-	62013	0.010	1.41	-

Fig. 4 GT performance of the LbCas12a variants at the SlHKT1;2 and SlEPSPS1 loci. a-b. Schematic diagrams describing the expected GT processes for exchanging the homologous DNA donor template with the genomic sequence at the SlHKT1;2 (**a**) and SlEPSPS1 (**b**) loci. The D217 coding sequence was added during the cloning of the HKTD1 donor for exchange with the N217 sequence of the genomic site. The lengths of homologous arms are shown. Two cutting sites (LbCas12a cutting sites 1 and 2) were planned to support the GT. The reverse and forward primers for amplifying the targeted sites by PCR are shown with black arrows. The I178 and S182 coding sequences were added during the cloning of the EPSPS1D3 donor for exchange with the T178 and P182 sequences of the genomic site. The lengths of homologous arms are shown. Two cutting sites (LbCas12a cutting sites 1 and 2) were used for the GT experiments. The reverse and forward primers for amplifying the targeted sites by PCR are shown with black arrows. In **b**, LbCas12a cutting site 2 is set as position 1, and the other positions are calculated accordingly. The diagrams were drawn not to their actual scales. **c.** The GT and indel mutation efficiencies assessed by targeted deep sequencing. At the SlHKT1;2 locus, four different crRNAs (single gRNAs: crR1.20^{HKT12}; crR2.20^{HKT12}, and dual gRNAs: crR1-2.20^{HKT12}; crR1.23^{HKT12}) were used for comparison of the LbCas12a variants in GT performance. A T-DNA vector was also used for comparison with the replicon system. With the SlEPSPS1 gene, only one dual gRNA construct (crR1-2.23^{EPSPS1}) was used with the two LbCas12a variants. Wt: wild-type LbCas12a; tt: ttLbCas12a.

Figure 5

a

Construct	LbCas12a variant	crRNA	Site 1			Site 2		
			Total read	GT efficiency (%)	Indel rate of gRNA1 (%)	Total read	GT efficiency (%)	Indel rate of gRNA3 (%)
pHRES2.9	wt	crR1-3.23^{EPSPS1}	117670	0.002±0.002	0.958±0.203	149673	0.009±0.002	1.339±0.233
pHRES2.10		crR1-3.23^{EPSPS1} + crR2-4.23^{EPSPS1}	105753	0.000	0.934±0.042	148166	0.004±0.003	1.235±0.079
pHRES2.11	tt	crR1-3.23^{EPSPS1}	109530	0.015±0.015	1.638±0.696	116243	0.018±0.009	2.712±0.629
pHRES2.12		crR1-3.23^{EPSPS1} + crR2-4.23^{EPSPS1}	107335	0.002±0.002	1.303±0.274	70779	0.007±0.002	1.867±0.283

b

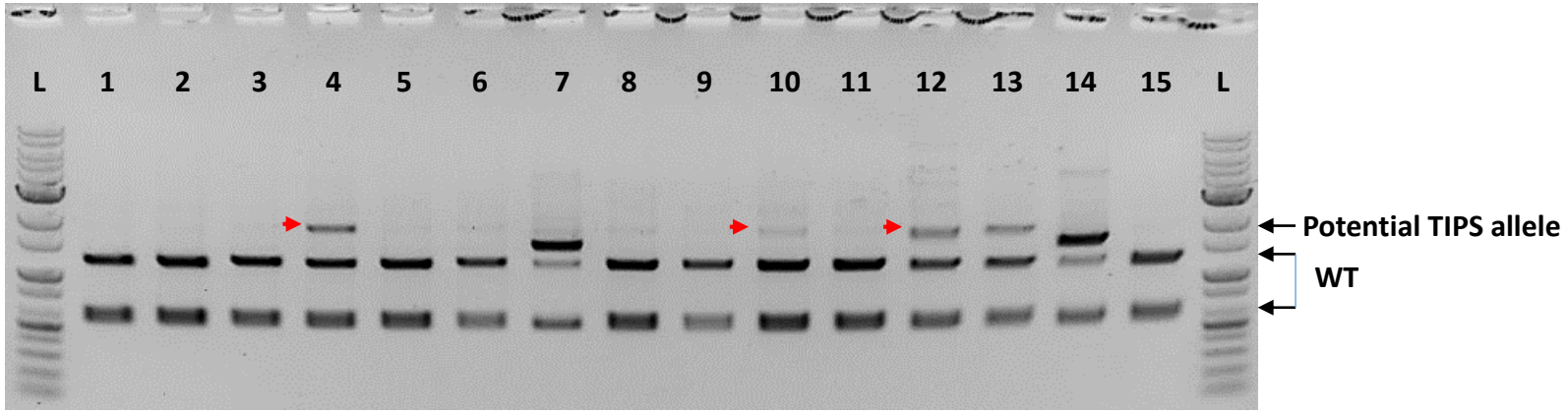

c

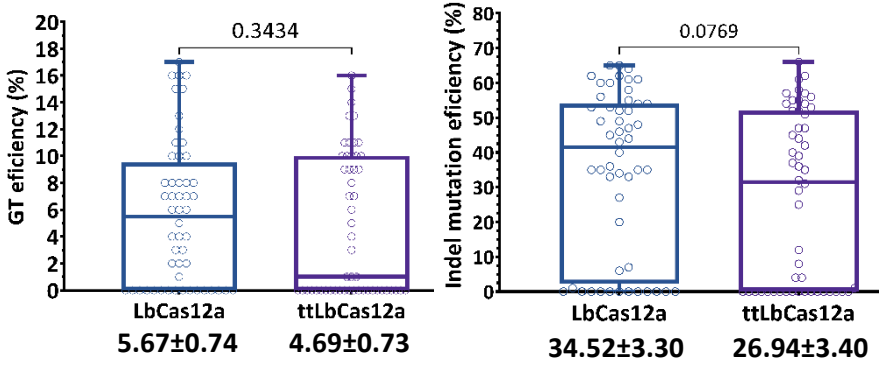

d

NU7441 treatment	Total read	GT efficiency (%)	Indel rate of gRNA1 (%)	Indel rate of gRNA2 (%)
0 μM	120904	0.006±0.003	3.425±1.106	1.549±0.903
1 μM	127254	0.009±0.005	3.069±0.629	1.502±0.510
2 μM	128950	0.004±0.002	2.918±0.619	1.476±0.454
3 μM	118501	0.002±0.001	3.440±0.983	1.633±0.560

Fig. 5 Further assessment of GT performance of the LbCas12a variants at the SlEPSPS1 locus. a. Assessment of GT efficiency by targeted deep sequencing with GT tools using two or four cutting sites with LbCas12a variants at the SlEPSPS1 locus. **b-c**. Indel mutation and GT efficiencies obtained with the LbCas12a variants at the plant stage. Fifty-two plants of each LbCas12a variant were obtained from the transformation of the GT tool with the crR1-2.23^{EPSPS1} expression cassette and used for PCR amplification of the targeted site with the UPEPSPS1-F2 and DNEPSPS1-R1 primers. In **b**, the PCR products were purified and screened for the potential GT allele by BpiI digestion since the BpiI site near the targeted site was modified in the DNA donor sequence. The red arrows indicate potential GT bands. 1-15: Representative transformants obtained from the transformation using the GT construct containing LbCas12a and crR1-3.23^{EPSPS1}. In **c**: All the purified PCR products were sequenced by the Sanger method, and the ab1 files were subsequently analyzed by ICE Synthego software to reveal the indel mutation and GT efficiencies. The indel mutation and GT efficiencies of all the samples were statistically analyzed using Student's t-test and plotted by GraphPad Prism version 9. The editing efficiencies (mean ± SEM) are shown at the bottom of each box. **d**. Targeted deep sequencing-mediated evaluation of NU7441 impacts on ttLbCas12a-based GT efficiency.